J Nanostruct 16(3): 4216-4233, Summer 2026

RESEARCH PAPER

Microwave-Assisted Graft Copolymerization of Chitosan-Based Porous Polymer Scaffolds for Controlled Piroxicam Release in Bone Tissue Engineering

Ansam K. Neamah, Nadia A. Hussein Al-Assady *

Department of Chemistry, College of Education for Pure Science, University of Basrah, Basrah, Iraq

ARTICLE INFO

Article History:
Received 12 March 2026
Accepted 21 June 2026
Published 01 July 2026

Keywords:
Chitosan
Drug delivery
Graphene oxide
Porous organic polymers
Tissue engineering

ABSTRACT

In this study, porous chitosan-based polymer scaffolds were successfully synthesized through microwave-assisted graft copolymerization of acrylamide and acrylic acid onto a chitosan backbone for potential bone tissue engineering and controlled drug delivery applications. Graphene oxide (GO) was incorporated into the polymeric matrix to improve the structural, mechanical, and physicochemical properties of the prepared scaffolds. In addition, piroxicam was loaded into the scaffolds to evaluate their controlled drug release performance. The prepared scaffolds were characterized using Fourier transform infrared spectroscopy (FTIR), swelling studies, porosity measurements, mechanical testing, in vitro drug release analysis, and degradation studies under oxidative and enzymatic physiological conditions. FTIR results confirmed the successful formation of the grafted polymer network and demonstrated intermolecular interactions between graphene oxide, the polymer matrix, and piroxicam molecules. The scaffolds exhibited interconnected porous structures, favorable swelling behavior, and good mechanical properties. The incorporation of graphene oxide significantly enhanced tensile and compressive strength due to increased cross-linking density and stronger intermolecular interactions. However, porosity and swelling behavior decreased slightly after GO incorporation because of reduced pore size and increased structural compactness. In vitro release studies demonstrated sustained and controlled release of piroxicam over an extended period. The presence of graphene oxide reduced the drug release rate and improved release stability. Furthermore, degradation studies revealed gradual and controlled oxidative and enzymatic degradation under simulated physiological conditions. Scaffolds containing graphene oxide exhibited improved structural stability and slower degradation behavior compared with pristine scaffolds. These findings suggest that the developed porous polymer scaffolds are promising candidates for bone tissue engineering and localized controlled drug delivery applications.

How to cite this article
K. Neamah A, A. Hussein Al-Assady N. Microwave-Assisted Graft Copolymerization of Chitosan-Based Porous Polymer Scaffolds for Controlled Piroxicam Release in Bone Tissue Engineering. J Nanostruct, 2026; 16(3):4216-4233. DOI: 10.22052/JNS.2026.03.103

* *Corresponding Author Email: ansam.khalidd@uobasrah.edu.iq*

This work is licensed under the Creative Commons Attribution 4.0 International License.
To view a copy of this license, visit http://creativecommons.org/licenses/by/4.0/.

INTRODUCTION

Bone injuries represent a significant clinical challenge in modern medicine and may arise from traumatic accidents, degenerative diseases, tumors, or chronic infections. Although bone possesses a natural capacity for regeneration, large defects or severe fractures often exceed the body's intrinsic healing ability. In such cases, medical intervention is required to restore structural integrity and functional recovery.

Conventional treatments for bone defects include autografts, allografts, and metallic implants. Despite their widespread use, these approaches present several limitations, such as donor site morbidity, limited availability of graft materials, risk of infection, and poor integration with surrounding tissues. Consequently, the development of advanced biomaterials capable of promoting bone regeneration has become a major focus in biomedical research [1].

Polymeric biomaterials have emerged as promising candidates for bone tissue engineering due to their tunable physicochemical properties, biocompatibility, and ability to mimic the extracellular matrix. Among these materials, chitosan has gained particular interest because of its biodegradability, non-toxicity, antimicrobial activity, and excellent biological compatibility. These properties make chitosan an attractive platform for the fabrication of scaffolds designed to support cell adhesion, proliferation, and tissue regeneration [2,3].

Porous polymer scaffolds play a crucial role in tissue engineering by providing a three-dimensional framework that facilitates nutrient diffusion, cell migration, and tissue formation. The structural characteristics of these scaffolds, including pore size, porosity, and mechanical stability, strongly influence their biological performance [4].

In recent years, researchers have focused on integrating drug delivery systems within polymeric scaffolds to enhance therapeutic outcomes. The incorporation of anti-inflammatory drugs into scaffolds can reduce post-surgical inflammation and improve the healing process [5,6]. Piroxicam Fig. 1, a non-steroidal anti-inflammatory drug (NSAID), is widely used for pain relief and inflammation control and has shown potential for localized delivery in tissue engineering applications [7].

Furthermore, the incorporation of nanomaterials such as graphene oxide (GO) into polymer matrices has been reported to improve mechanical strength, surface properties, and biological activity. Graphene oxide provides functional groups that enhance interactions with polymer chains and biomolecules, thereby improving scaffold performance [8].

Therefore, the present study aims to synthesize a porous chitosan-based graft copolymer scaffold using microwave-assisted polymerization with acrylate monomers. Additionally, graphene oxide is incorporated to enhance the scaffold's structural properties, while piroxicam is loaded to investigate controlled drug-release behavior. The resulting material is evaluated as a potential multifunctional scaffold for bone tissue engineering and localized drug delivery.

MATERIALS AND METHODS

Chemicals

B.D.H., England supplied Chitosan (50%). Acrylic acid was supplied by Fluka, Switzerland. Sodium hydroxide was supplied by Aldrich, Germany. Acrylamide (AM) was supplied by Sigma-Aldrich, Germany. Acetic acid solution (2%) was supplied by Aldrich, Germany. Sodium persulfate (APS) was supplied by Fluka, Switzerland. Tetramethylethylene diamine (TEMED) was

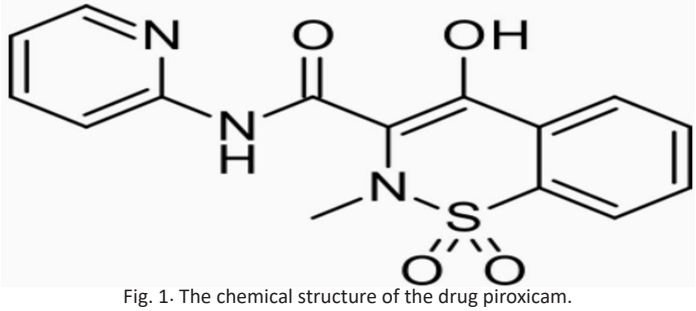


Fig. 1. The chemical structure of the drug piroxicam.

CC BY

supplied by Merck, Switzerland. The two solvents, methanol (from GCC, UK) and ethanol (from Scharal, Spain), were supplied. All other chemicals were of sufficient purity for use in chemical analysis.

Methods

Preparation of Porous Organic Polymer (CAAm Scaffold)

The porous organic polymer (CAAm scaffold) was synthesized via a two-step procedure involving monomer solution preparation followed by chitosan-based free radical polymerization.

Monomer Solution Preparation

Acrylic acid (AA, 6 g) was partially neutralized by dissolving in 12.5 mL of 5 M sodium hydroxide under ice-bath conditions for 5 min. Separately, acrylamide (AM, 6 g) was dissolved in 12 mL of distilled water under continuous stirring until a clear solution was obtained. N, N'-methylenebisacrylamide (MBA, 0.043 g), used as a crosslinking agent, was dissolved in 5 mL of distilled water. The AM and MBA solutions were subsequently mixed and then added dropwise to the neutralized AA solution under continuous stirring to form a homogeneous monomer mixture.

Chitosan Solution Preparation

Chitosan (1 g) was dissolved in 40 mL of 2% (v/v) acetic acid solution under constant stirring until complete dissolution was achieved.

Initiation and Polymerization

Ammonium persulfate (APS, 0.118 g) and N, N, N', N'-tetramethylethylenediamine (TEMED, 0.118 g) were separately dissolved in 5 mL of distilled water each. The initiator system (APS/TEMED) was then added dropwise to the chitosan solution at 60°C under continuous stirring and maintained for 10 min to activate the reaction medium. After cooling to room temperature, the previously prepared monomer mixture was added dropwise to the chitosan solution under continuous stirring.

Gel Formation and Post-Treatment

The resulting reaction mixture was transferred into a glass vessel and subjected to microwave irradiation at 400 W for 1–2 min, leading to the formation of a yellow hydrogel. The obtained gel was cut into small pieces and thoroughly washed with methanol several times, including overnight soaking, to remove unreacted monomers and impurities. Subsequently, the samples were rinsed with ethanol and dried in an oven at 60°C

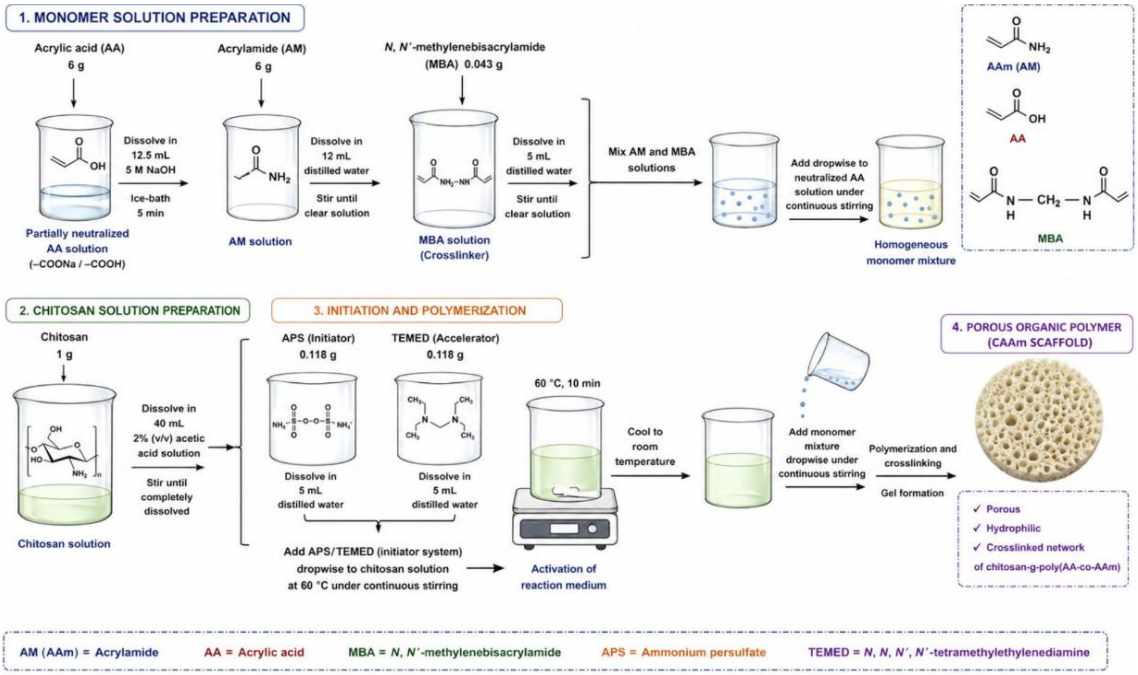


Fig. 2. Reaction scheme for the synthesis of CAAm hydrogel.

CC BY

for several hours until a constant weight was achieved, yielding the final porous CAAm scaffold.

Preparation of Porous Organic Polymer Network Incorporating Graphene Oxide (CAAm/GO)

The porous organic polymer network incorporating graphene oxide (CAAm/GO) was synthesized following the same procedure described for the pristine polymer network. Briefly, 0.5 g of graphene oxide (GO) was incorporated into the chitosan solution during its preparation in acetic acid under continuous stirring to ensure homogeneous dispersion. Subsequently, the resulting GO–chitosan mixture was combined with the pre-prepared monomer solution, and the polymerization process was carried out under identical conditions. All subsequent steps were performed as previously described to obtain the final porous CAAm/GO polymer network.

Preparation of Porous Organic Polymer Networks Loaded with Drug

The drug loading was performed using an optimized post-synthesis diffusion method to ensure maximum loading efficiency while preserving both the structural integrity of the polymer network and the chemical stability of the drug.

Briefly, 100 mg of the dried porous polymer network was immersed in 10 mL of a freshly prepared ethanolic solution containing 10 mg of Piroxicam. The hydrogel was allowed to swell fully in the drug solution to facilitate diffusion into the internal porous structure.

The system was maintained under gentle shaking (100 rpm) at room temperature for 24 h to achieve equilibrium loading. To further enhance drug uptake, the loading process can be conducted under mild vacuum conditions or by applying intermittent sonication to improve penetration of the drug into micropores.

After loading, the hydrogel was removed and lightly rinsed with distilled water to eliminate loosely bound drug molecules from the surface without affecting the entrapped fraction. The sample was then dried at ambient conditions until a constant weight was reached.

Analytical Methods

Morphological Study

The polymer scaffolds were imaged using a digital light microscope. They were also examined using a high-resolution microscope.

Fourier Transform Infrared Spectroscopy

The Fourier transform infrared spectra of the drug, the polymer scaffolds alone, and the drug-loaded polymer scaffolds were recorded using a Fourier transform infrared spectrometer (model 4100 type A, Perkin-Elmer, Norwalk, CT, USA) with potassium bromide tablets (400–4000 cm^{-1}).

X-ray Diffraction (XRD) Phase Analysis

X-ray diffraction (XRD) was used (using a Philips X'Pert-MPD system at a CoKa wavelength of 1.5418 angstroms) to analyze the structure of the porous organic network structures prepared from Ce/Am/AA. The diffraction meter was operated at 40 kV and 40 mA within a 2ε range of 5 to 69.99°, using a step of 1.000 s.

In vitro release studies

Briefly, 100 mg of the prepared polymer scaffolds with the drug were placed in artificial dialysis bags and immersed in 100 mL of phosphate buffer at pH 7.4 after being fixed in sterile beakers. The beakers were carefully covered with a glass lid and placed on a magnetic motor at 100 rpm at 37 ± 1 °C. Four mL of the solvent were withdrawn at regular intervals and replaced with fresh solvent. The samples were analyzed spectroscopically at 354 nm to determine the concentration of the dissolved drug (drug content) using UV spectroscopy. All experimental units were analyzed three times (n=3) [9,10].

Mechanical Properties Testing

The tensile properties of the structures were measured according to ASTM D638-98. The test was performed using an Instron test apparatus equipped with a 5-lb load cell. A moving head speed of 10 mm/min was used. The structure was cut longitudinally and subjected to testing. The samples were evaluated.

In Vitro Degradation of Polymer Scaffolding Structures

In Vitro Degradation Studies

Oxidative Degradation Study

The oxidative degradation behavior of the prepared polymeric scaffolds was evaluated using a reactive oxidation system based on Cobalt (II) chloride and Hydrogen peroxide.

Briefly, a 0.1 M cobalt chloride solution was

CC BY

prepared and used as a catalyst for the generation of reactive oxygen species. A 30% (v/v) hydrogen peroxide solution was diluted with distilled water to obtain a final concentration of 20% (v/v). The diluted hydrogen peroxide was then gradually added to the cobalt chloride solution under continuous magnetic stirring.

The resulting dark blue oxidation solution was stirred until a homogeneous mixture was obtained. This system promotes the formation of highly reactive radicals (e.g., hydroxyl radicals), which accelerate oxidative degradation of the polymer matrix.

The prepared oxidation solution was then distributed into separate containers, ensuring sufficient volume to fully immerse each scaffold sample. The samples were incubated under controlled conditions, and degradation behavior was monitored over time [11].

Enzymatic Degradation (Hydrolysis) Using Lysozyme

Enzymatic degradation of the polymeric scaffolds was investigated using Lysozyme to simulate physiological hydrolytic conditions.

A lysozyme solution was prepared by dissolving 0.15 g of lysozyme in 100 mL of phosphate-buffered saline (PBS, pH 7.4). The PBS solution was used to maintain a stable physiological pH environment. The mixture was gently stirred using a magnetic stirrer until complete dissolution of the enzyme was achieved, yielding a clear and homogeneous solution.

The prepared lysozyme solution was transferred into sterile containers, ensuring adequate volume for complete immersion of each scaffold sample. The samples were then incubated under physiological-like conditions to evaluate enzymatic degradation behavior over time[12].

Lysozyme specifically promotes the degradation of polysaccharide-based components (such as chitosan) through cleavage of glycosidic bonds, thereby contributing to the breakdown of the scaffold structure.

Scaffold Porosity

The porosity of the prepared polymer network was investigated using the liquid displacement method. Ethanol was used as the displacement fluid in this procedure due to its ease of penetration into the pores of the polymer scaffold structure. A dry scaffold was placed in a graduated cylinder filled with a predetermined volume (V1) of ethanol, and the cylinder was then placed in a vacuum for 20 minutes to allow the ethanol to penetrate the scaffold pores. The total volume of ethanol contained in the sample was recorded as V2. The scaffold was then removed from the graduated cylinder, and the remaining volume of ethanol was recorded as V3. The amount of open pores in the scaffold, P(%), was calculated according to the following equation:

$$P\,(\%) = (V_1 - V_3)/(V_2 - V_3) \times 100\% \quad (1)$$

where (V2–V3) = total volume of the scaffold and (V1–V3) = volume of ethanol retained in the sample. Three specimens of the sample were used for the porosity measurements, and the results were averaged [13].

Equilibrium Swelling Studies of Scaffolds

The % water absorbed by the scaffolds was studied by soaking them overnight in distilled water at room temperature. The% water absorbed was calculated from the following equation

$$\text{Equilibrium swelling} = \frac{W_f - W_i}{W_i} \times 100 \quad (2)$$

where Wi is the initial weight of scaffold formulations (mg), and Wf is the weight of scaffold formulations (mg) after soaking the water until saturation (after 24 hours) [14].

RESULTS AND DISCUSSION

Characterization of the Prepared Polymeric Scaffolds

FTIR Analysis

Fourier Transform Infrared Spectroscopy (FTIR) was employed to confirm the successful formation of the prepared polymeric scaffold and to investigate the interaction between the polymer matrix and the loaded drug (piroxicam). The obtained spectra revealed several characteristic absorption bands corresponding to the functional groups of chitosan and acrylamide, indicating the successful formation of the polymer network.

Fig. 3 presents the FTIR spectrum of the synthesized CAAm scaffold, confirming the successful formation of the chitosan-g-poly(acrylamide-co-acrylic acid) network.

A broad absorption band observed at 3351 cm^{-1} is attributed to the overlapping stretching

vibrations of O–H and N–H groups originating from chitosan and acrylamide. The broadness of this peak indicates extensive hydrogen bonding interactions within the polymeric matrix, which contribute significantly to the stability of the three-dimensional network. A distinct band at 3182 cm^{-1} corresponds to the N–H stretching vibration of amide groups, confirming the successful incorporation of acrylamide units into the scaffold structure. The absorption bands at 2930 cm^{-1} and 2859 cm^{-1} are assigned to aliphatic C–H stretching vibrations, characteristic of the polymer backbone. A strong peak at 1660 cm^{-1} is attributed to the C=O stretching vibration (Amide I), while the band at 1560 cm^{-1} corresponds to N–H bending (Amide II). The presence of these peaks provides strong evidence for the formation of amide linkages and confirms successful graft polymerization. Additionally, the bands at 1399 cm^{-1} and 1310 cm^{-1} are assigned to C–H bending and C–N stretching vibrations, respectively, further supporting the formation of the polymeric amide network. The peaks observed at 1171 cm^{-1}, 1111 cm^{-1}, and 1027 cm^{-1} correspond to C–O and C–O–C stretching vibrations associated with the glycosidic linkages of chitosan. The presence of these peaks indicates that the chitosan backbone remains structurally intact after polymerization.

Importantly, the absence of significant peak shifting or disappearance in the characteristic chitosan bands suggests that the polymerization process occurred via grafting rather than backbone degradation. Moreover, the simultaneous presence of amide and polysaccharide peaks confirms the successful formation of an interpenetrating polymer network structure.

Overall, the FTIR results confirm the successful synthesis of a chemically integrated chitosan-based porous scaffold via graft copolymerization of acrylamide, while preserving the structural integrity of the native biopolymer.

The FTIR spectrum of Piroxicam [15] exhibits several characteristic absorption bands corresponding to its functional groups, shown in Fig. 4. A broad band observed at 3330 cm^{-1} is attributed to the stretching vibrations of O–H and/or N–H groups, which are involved in intramolecular hydrogen bonding within the drug

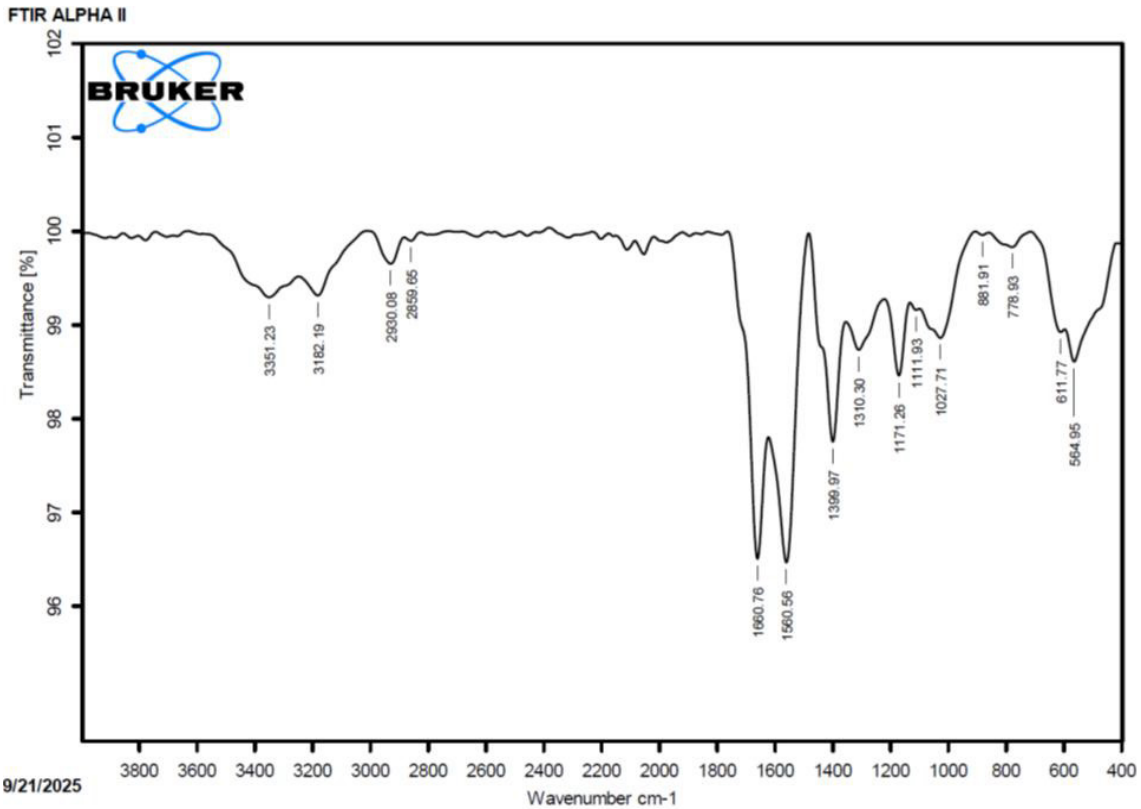


Fig. 3. Spectrum of the prepared polymer network (CAAm Scaffolds).

CC BY

structure. The band at 2926 cm^{-1} corresponds to the aliphatic C–H stretching vibrations. A prominent peak at 1631 cm^{-1} is assigned to the C=O stretching vibration of the amide group, representing one of the key characteristic features of piroxicam.

The absorption band at 1525 cm^{-1} is attributed to N–H bending vibrations (amide II), along with contributions from aromatic ring vibrations. Bands appearing at 1344 cm^{-1} and 1298 cm^{-1} are characteristic of asymmetric and symmetric stretching vibrations of the sulfonamide group (S=O), confirming the presence of this functional group in the molecular structure. Furthermore, the bands in the region 1133–1019 cm^{-1} are assigned to C–N and C–O stretching vibrations.

The peaks at 868 cm^{-1}, 830 cm^{-1}, and 767 cm^{-1} correspond to out-of-plane bending vibrations of aromatic C–H bonds, indicating the presence of substituted aromatic rings.

The FTIR spectrum, Fig. 5 of the drug-loaded scaffold (CAAm/Piroxicam), shows noticeable changes compared to both the pristine scaffold and the pure drug, indicating successful drug incorporation and interaction with the polymeric network. A broad absorption band at 3337 cm^{-1} is attributed to overlapping O–H and N–H stretching vibrations. The increased intensity and slight broadening of this band compared to the unloaded scaffold suggest enhanced hydrogen bonding interactions between piroxicam molecules and the hydroxyl and amino groups of chitosan. The band observed at 3195 cm^{-1} corresponds to N–H stretching vibrations, confirming the coexistence of amide groups from both acrylamide and piroxicam within the system. A characteristic peak at 1663 cm^{-1} is assigned to C=O stretching (Amide I). The slight shift in this peak relative to both the pure polymer and pure drug indicates molecular-level interactions, most likely hydrogen bonding or dipole–dipole interactions between the drug and the polymer matrix. Similarly, the band at 1555 cm^{-1} (Amide II, N–H bending) further confirms the presence of amide functionalities and supports successful drug incorporation. The peaks at 1445 cm^{-1} and 1400 cm^{-1} are attributed to C–H bending and C–N stretching vibrations, respectively, consistent with the polymeric backbone. The bands at 1158 cm^{-1} and 1027 cm^{-1} correspond to C–O and C–O–C stretching vibrations of the chitosan backbone, indicating that the polysaccharide structure remains intact after drug loading. Importantly, the appearance of a band at 762 cm^{-1}, characteristic of aromatic C–H out-of-plane bending, confirms the presence of the aromatic structure of piroxicam within the

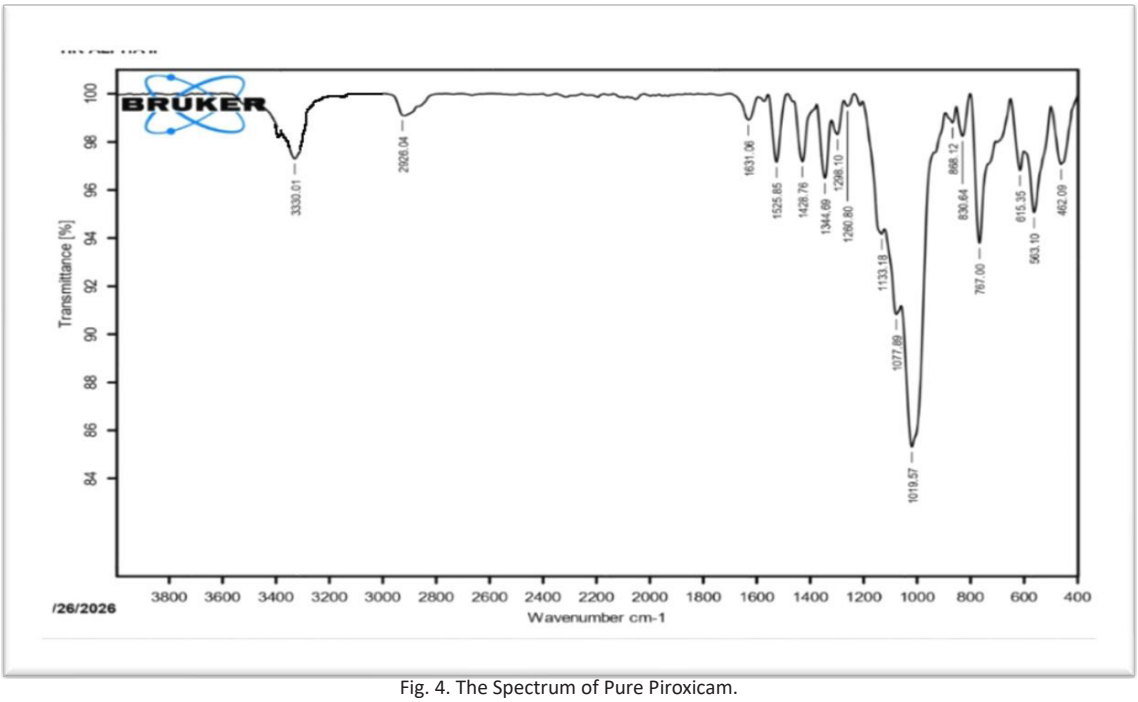


Fig. 4. The Spectrum of Pure Piroxicam.

CC BY

scaffold.

The observed peak shifts and intensity changes—particularly in the O–H/N–H and C=O regions—indicate that the drug is not merely physically adsorbed but interacts with the polymer network through hydrogen bonding and secondary interactions.

The FTIR results confirm the successful loading of piroxicam into the CAAm scaffold and suggest that drug incorporation occurs through a combination of physical entrapment and intermolecular interactions, which are expected to influence the drug release behavior.

The FTIR spectrum of the CAAm/GO composite scaffold exhibits several significant changes compared to the pristine CAAm hydrogel,

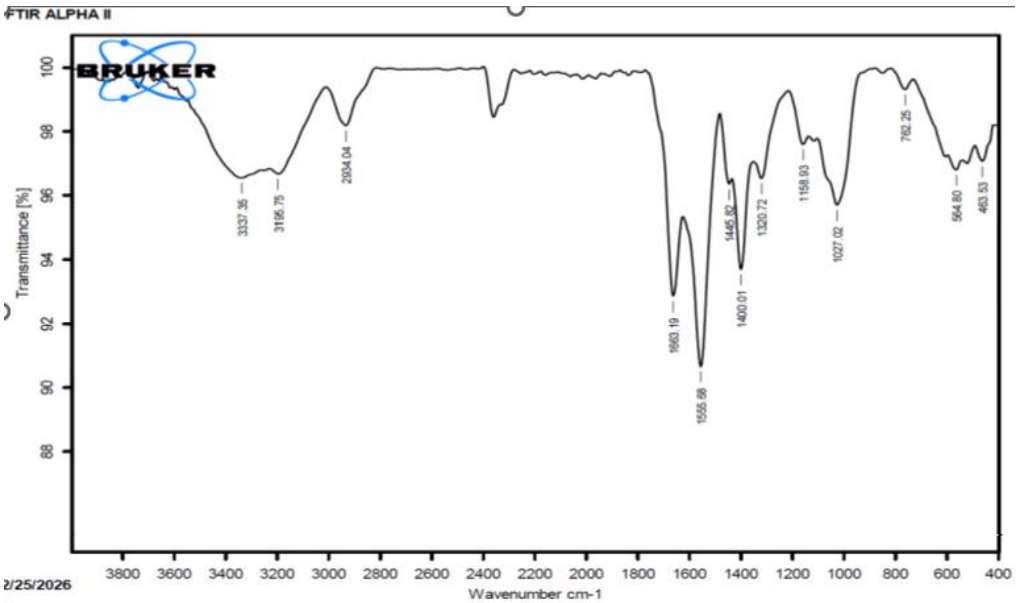


Fig. 5. Polymer Network Spectrum (CAAm Scaffolds) After Piroxicam Loading.

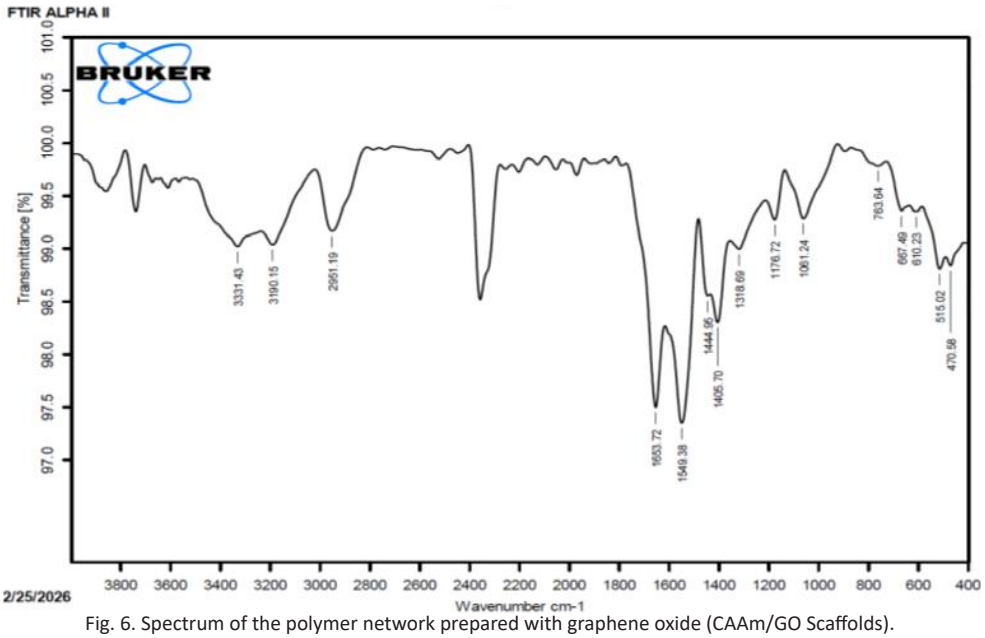


Fig. 6. Spectrum of the polymer network prepared with graphene oxide (CAAm/GO Scaffolds).

CC BY

confirming the successful incorporation of graphene oxide (GO) into the polymeric network. A broad absorption band in the region 3331–3190 cm^{-1} is observed, corresponding to overlapping O–H and N–H stretching vibrations. The increased broadness and intensity of this band indicate enhanced hydrogen bonding interactions, which arise from the abundant oxygen-containing functional groups (–OH and –COOH) present on the GO nanosheets. These groups interact strongly with the hydroxyl and amino groups of chitosan as well as amide groups in the polymer network. The characteristic amide I (C=O) band shows a slight shift from approximately 1660 cm^{-1} to 1653 cm^{-1}, suggesting the formation of intermolecular interactions between GO and the polymer chains. This shift is typically associated with hydrogen bonding or dipole–dipole interactions, indicating partial electronic interaction between GO sheets and the polymer matrix. Additionally, the preservation of amide II and other characteristic polymer peaks confirms that the fundamental structure of the CAAm network remains intact after GO incorporation. New absorption bands appearing in the region 763–470 cm^{-1} are attributed to skeletal vibrations and aromatic lattice modes of GO, providing further evidence of its successful integration within the scaffold.

The observed peak broadening and shifting—particularly in the O–H/N–H and C=O regions—indicate that GO is not merely physically dispersed but actively participates in the network through strong intermolecular interactions, effectively acting as a secondary crosslinking agent within the hydrogel system. These spectral modifications confirm the successful formation of a chemically interactive CAAm/GO composite hydrogel, where graphene oxide enhances network stability and introduces additional functional sites that are expected to improve adsorption and drug delivery performance.

X-Ray Diffraction (XRD)

X-ray diffraction (XRD) results showed a clear difference between the CAAm scaffold Fig. 7 and the CAAm/GO scaffold Fig. 8. The graphene oxide-free scaffold exhibited sharp, well-defined peaks at 2θ angles of approximately 27.5°, 31.8°, 45.5°, 56.5°, 66.3°, and 75.4°, indicating the presence of semi-crystalline regions resulting from the relative ordering and compaction of the chitosan-acrylamide chains due to hydrogen bonding between hydroxyl, amine, and amide groups. The main peak at 31.8° was the most intense, demonstrating a clear structural order within parts of the polymer network. After the addition of graphene oxide, most of these sharp peaks disappeared, and a broad diffraction band appeared, centered at approximately 20–25°, with weak residual reflections at around 31–32° and

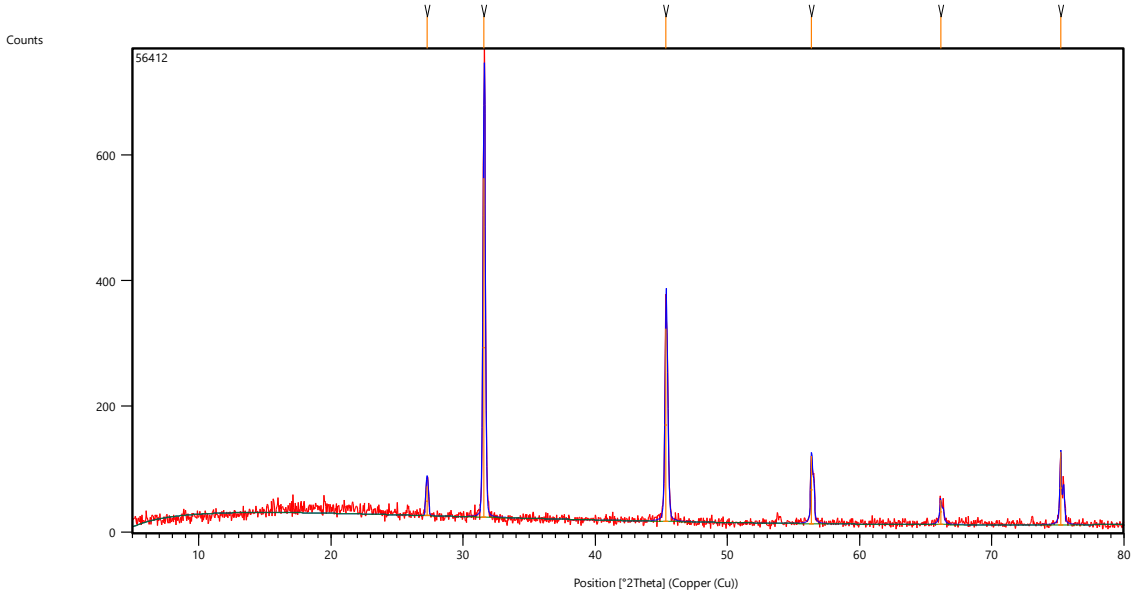


Fig. 7. Results of X-ray diffraction analysis of the prepared polymer network structure (CAAm scaffold).

CC BY

39–40°. This indicates a decrease in crystallinity and a shift towards a more irregular lattice structure.

The disappearance of the crystalline peaks does not necessarily imply increased porosity or swelling; rather, it indicates a disruption of the regular alignment of the polymer chains. In this study, the introduction of graphene oxide led to a large number of interactions between the functional groups on its surface (-OH,-COOH, and epoxy) and between the amine and hydroxyl groups in chitosan and the amide groups in acrylamide, resulting in a more cohesive and tightly bound lattice. Consequently, the mobility of the polymer chains decreased, and the free volume within the scaffold was reduced, despite the apparent decrease in crystallinity as measured by XRD.

This interpretation is directly reflected in the porosity and swelling results. The increased cross-linking density resulting from the presence of graphene oxide led to a reduction in the size and

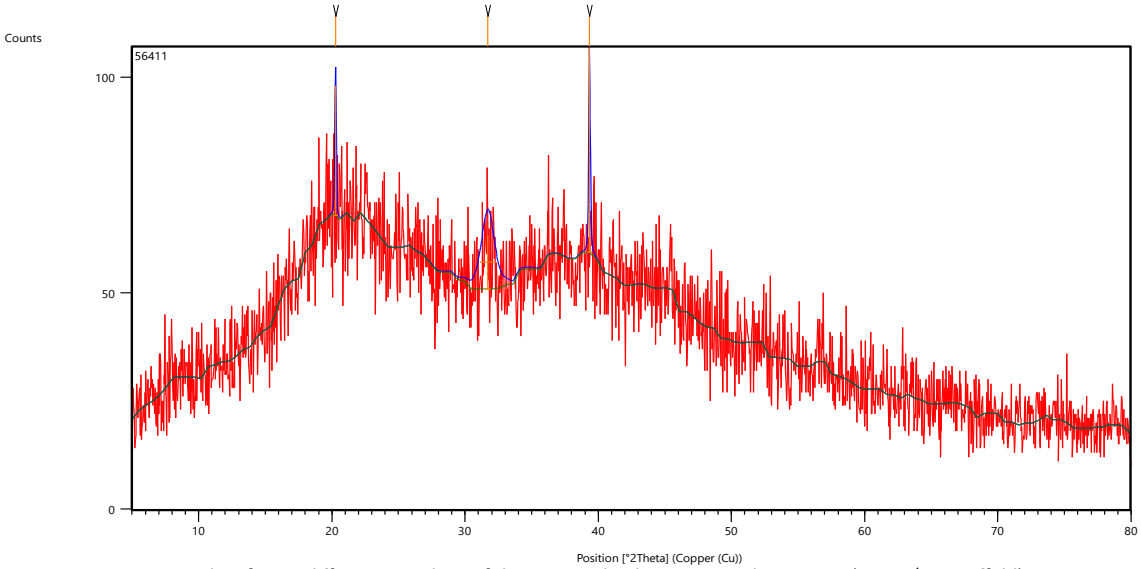


Fig. 8. Results of X-ray diffraction analysis of the prepared polymer network structure (CAAm/GO scaffold).

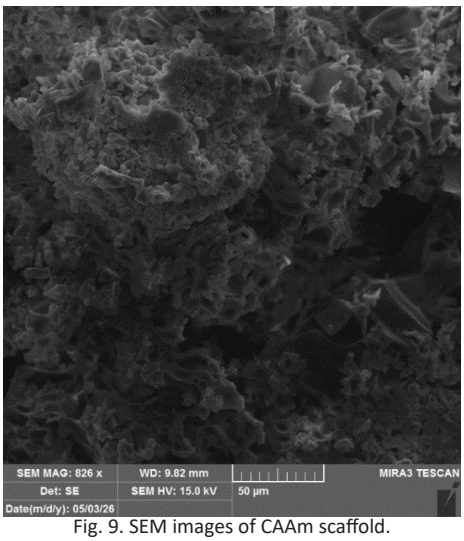


Fig. 9. SEM images of CAAm scaffold.

CC BY

number of internal spaces within the scaffold, which explains the significant decrease in porosity compared to the unloaded scaffold. Furthermore, the tightness of the polymer network limited the penetration of water molecules into the structure, resulting in a decrease in swelling. Thus, the XRD, porosity, and swelling results are not contradictory but rather complementary. While XRD indicates a decrease in crystallinity due to chain disorder, the porosity and swelling results indicate that this disorder was accompanied by an increase in network cohesion, not an increase in internal spaces.

Accordingly, the XRD results confirm that the addition of graphene oxide led to a decrease in crystallinity and the disappearance of the sharp peaks at 27.5°, 31.8°, 45.5°, and 56.5°. However, this decrease was accompanied by an increase in cross-linking density and internal cohesion of the scaffold, which practically resulted in a decrease in porosity and swelling and a slower drug release. These results indicate the success of graphene oxide in improving scaffold stability and controlling its pharmacological behavior, properties required in polymer scaffold applications for textile engineering and sustained drug release systems.

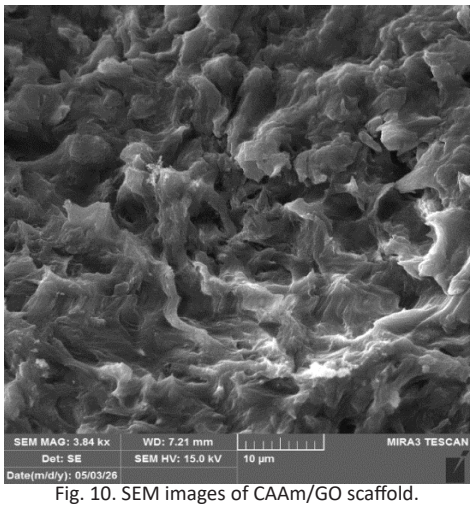


Fig. 10. SEM images of CAAm/GO scaffold.

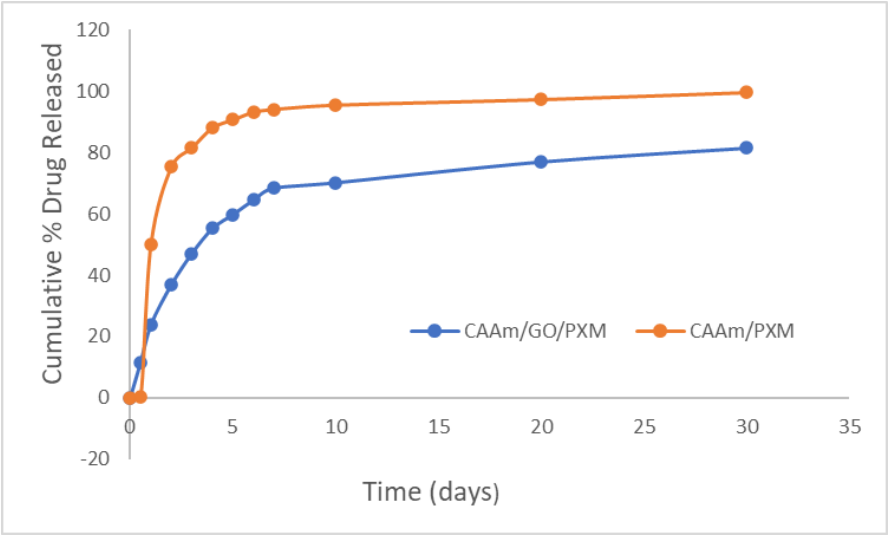


Fig. 11. Average percentage piroxicam release from different Scaffolds.

CC BY

Scanning Electron Microscopy Analysis

Scanning electron microscopy (SEM) images, as shown in Fig. 9, revealed that the CAAm network possessed an open porous structure with interconnected spaces and larger pore sizes. In contrast, the introduction of graphene oxide resulted in a more compact and less porous structure, shown in Fig. 10. This behavior is attributed to the strong interactions between the functional groups of graphene oxide and the amine and hydroxyl groups in chitosan and the amide groups in acrylamide, leading to increased cross-linking density within the polymer network and reduced interchain spacing. Furthermore, the graphene oxide sheets acted as nanofillers within the polymer spaces, resulting in a decrease in the size and number of pores observed in the SEM images. This impacted the functional properties of the scaffold, with reduced porosity and swelling, and a slower drug release rate due to increased resistance to water and molecule transport through the polymer network.

In vitro piroxicam release study from scaffolds

Fig. 11 illustrates the cumulative release profile of the prepared polymer scaffolds in phosphate-buffered solution (pH 7.4) at 37°C. The release curves exhibit an initial burst followed by sustained, controlled release behavior. The structural characteristics of the prepared porous organic polymer network mainly govern this release pattern.

The amorphous structure and high porosity of the network facilitate water penetration into the scaffold, enabling the gradual diffusion of drug molecules. Consequently, a relatively slow and uniform release profile is achieved over an extended period. In addition, progressive relaxation of the polymer chains contributes to further drug liberation with time.

Therefore, the release of piroxicam from the prepared hydrogel occurs through a combined mechanism involving diffusion, swelling, and polymer chain relaxation. The amorphous morphology and enhanced porosity promote the uptake of the aqueous medium, whereas hydrogen bonding interactions between the drug molecules and the functional groups of the hydrogel help minimize sudden drug release. This behavior provides a sustained-release system suitable for pharmaceutical and drug delivery applications.

The drug release was evaluated using the following definitions:

$$\text{Drug Release (\%)} = \frac{\text{Amount of drug release (mg)}}{\text{Total amount of loaded (mg)}} \times 100 \quad (3)$$

The incorporation of graphene oxide significantly reduced the drug release rate due to the increase in physical cross-linking density and the reduction in pore size within the polymer network. These structural modifications enhanced the stability of the hydrogel matrix and restricted the diffusion of drug molecules, leading to a more controlled and sustained release behavior. Consequently, the graphene oxide-containing system exhibited improved release stability and prolonged drug delivery performance.

Mechanical and Porous Properties

The compressive modulus is one of the most important mechanical parameters used in the design and evaluation of scaffolds and engineered tissues. It reflects a material's ability to resist deformation under compressive loads and directly influences cell behavior, new tissue formation, and the matching of mechanical properties to natural tissue.

The researchers stated that determining the modulus of elasticity and the compressive modulus of engineered scaffolds is of fundamental importance in tissue engineering because the mechanical behavior is closely linked to the biological properties of implanted tissues and scaffolds[16]. Table 1 presents the mechanical properties of the prepared porous organic polymer network structures. The mechanical tests demonstrated that the prepared hydrogel possesses moderate tensile strength combined with high elongation, indicating the flexibility of the polymer network. In addition, the hydrogel exhibited good compressive strength due to the three-dimensional arrangement of the polymer chains.

Moreover, the incorporation of graphene oxide improved both the compressive and tensile strength of the prepared structures. This enhancement can be attributed to the increased cross-linking density, improved stress transfer throughout the polymer matrix, and the formation of strong hydrogen-bonding interactions between the functional groups of graphene oxide and the polymer chains.

The porosity of the prepared structures was

CC BY

evaluated using the liquid displacement method. Ethanol was selected as the displacement medium because of its ability to easily penetrate the pores of the prepared scaffold structure without causing swelling or shrinkage. The porosity values of the polymeric structures were subsequently calculated and are summarized in Table 1.

The chemical cross-linking within the three-dimensional acrylamide network, together with the hydrogen-bonding interactions between the amino and hydroxyl groups of chitosan and the amide groups of acrylamide, as well as the difference in solubility between the two polymers, collectively contribute to the formation of internal voids within the hydrogel matrix. This heterogeneous interpenetrating network structure provides the prepared hydrogel with a porous and interconnected morphology.

Upon incorporation of graphene oxide into the polymer network, the porosity of the prepared hydrogel decreases due to the increased cross-linking density, partial filling of the internal voids by graphene oxide nanosheets, and the formation of additional hydrogen-bonding interactions between graphene oxide and chitosan chains. These structural changes are consistent with the observed enhancement in mechanical properties and the reduction in swelling behavior, as presented in the table.

Swelling Behavior of Structures at Equilibrium

The swelling behavior of the prepared structures at equilibrium was investigated as a function of time by immersing the samples in a fixed volume of distilled water under acidic (pH = 2) and alkaline (pH = 12) conditions at a temperature of 30 ± 5 °C. At predetermined time intervals, the samples were removed from the solution, gently blotted with filter paper to eliminate excess surface water, and then weighed to determine the swelling percentage. The equilibrium swelling ratio of the prepared structures was evaluated over a period of 24 hours.

The prepared hydrogel exhibited a high swelling capacity in a neutral medium, ranging between (430-698.1%). This behavior can be attributed to the hydrophilic nature of the polymer components, which contain functional groups

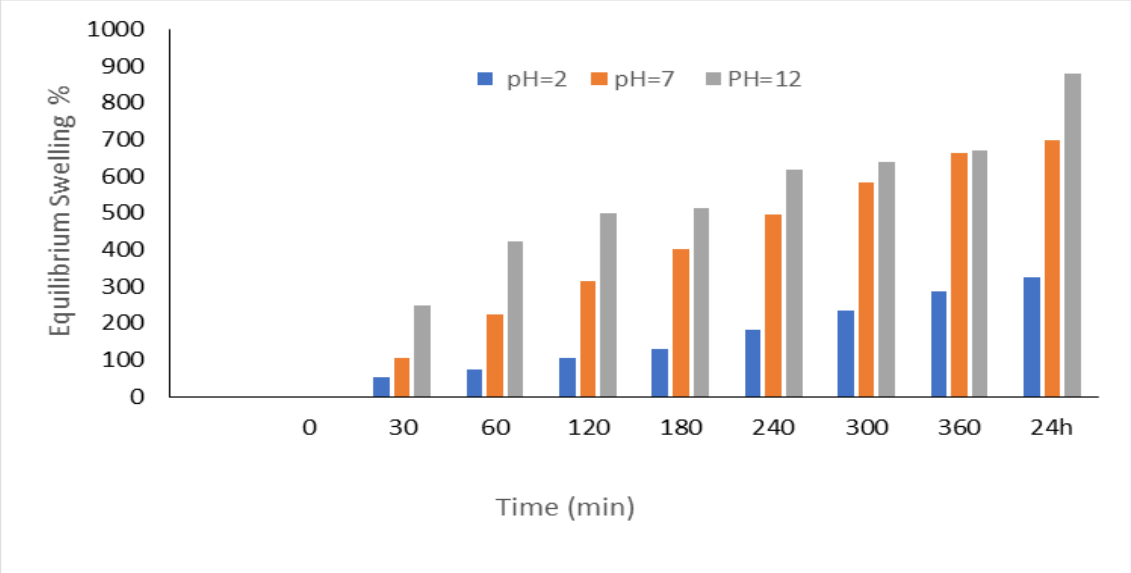


Fig. 12. Equilibrium Swelling of porous organic polymer network (CAAm Scaffolds).

Table 1. Mechanical properties and porosity of scaffolds.

Scaffolds Types	Tensile Strength $\sigma_{(Mpa)}$	Compressive Strength σ_M (Mpa)	Porosity %
CAAm Scaffolds	1.5	3.0	81
CAAm/GO Scaffolds	2.4	4.8	69

CC BY

capable of absorbing and retaining water within the network structure, including hydroxyl (-OH) and amino (-NH_2) groups in chitosan, as well as amide (-$CONH_2$) groups in acrylamide. In addition, the porous architecture of the polymer network facilitates water diffusion and storage within the hydrogel matrix.

Furthermore, the swelling capacity increased significantly in the alkaline medium due to the ionization of carboxylic groups, resulting in electrostatic repulsion between polymer chains and subsequent expansion of the network structure. In contrast, swelling decreased in the acidic medium because of the formation of ionic and hydrogen-bonding interactions between the protonated amino groups (-NH_3^+) and carboxylic groups (-COOH), leading to contraction of the polymer network and reduced water uptake.

For the scaffold prepared in the presence of graphene oxide, the calculated swelling values revealed a noticeable decrease in swelling behavior under different pH conditions. This reduction in swelling can be attributed to the increased physical entanglement within the polymer network, decreased porosity, and enhanced mechanical rigidity resulting from the

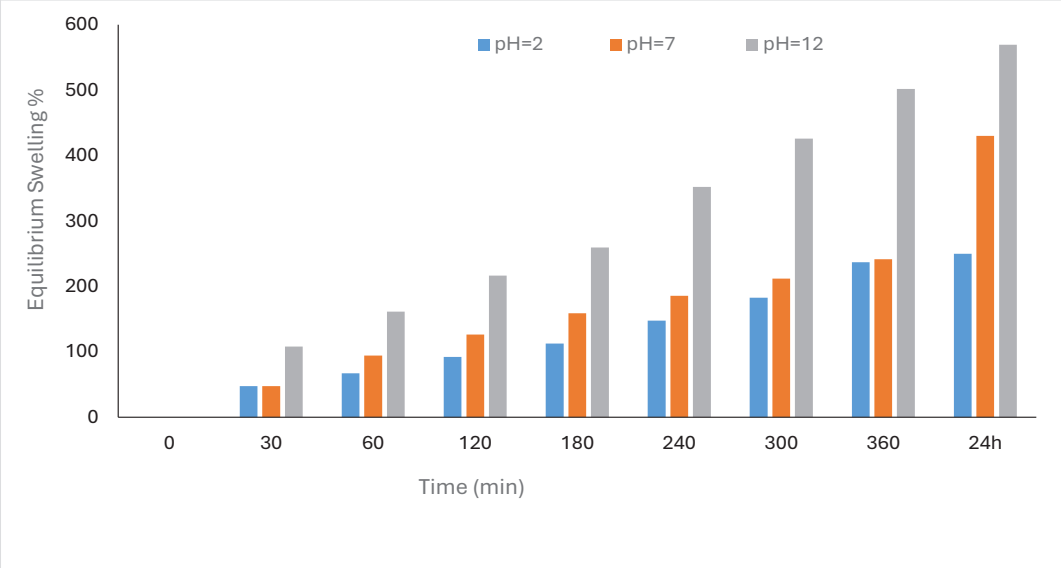


Fig. 13: Equilibrium Swelling of porous organic polymer network (CAAm /GO Scaffolds).

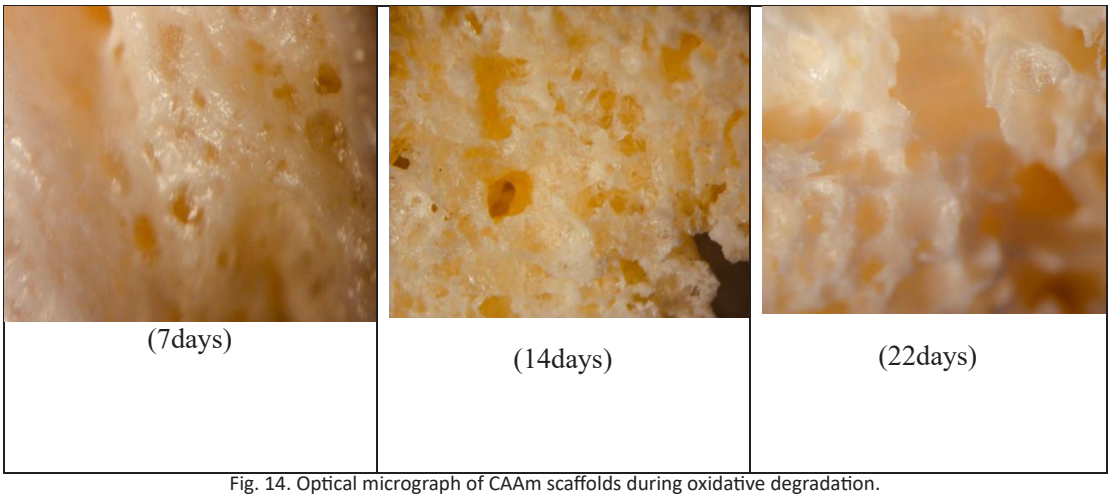


Fig. 14. Optical micrograph of CAAm scaffolds during oxidative degradation.

CC BY

incorporation of graphene oxide. In addition, the formation of stronger intermolecular interactions and hydrogen bonding between graphene oxide and the polymer chains restricts the mobility of the network and limits water uptake, thereby reducing the overall swelling capacity of the scaffold.

Degradation of Prepared Scaffolds

The degradation behavior of the prepared scaffolds represents a critical aspect of biomaterials research [17], as it provides valuable insight into their performance, stability, and durability under physiological conditions. In addition, degradation analysis is essential for evaluating the suitability of these scaffolds for biomedical applications such as tissue engineering and controlled drug delivery systems.

In this study, the prepared scaffolds were subjected to sequential incubation under controlled degradation environments. Comprehensive in vitro degradation experiments were conducted to investigate the stability and degradation characteristics of the polymeric scaffolds under simulated physiological conditions. The study mainly focused on two degradation mechanisms: oxidative degradation and enzymatic degradation.

The degradation behavior of the prepared scaffolds in oxidative media demonstrated distinct responses depending on the scaffold composition. The degradation process was monitored using the results presented in Figs. 14 and 15, together with light microscope observations of the scaffold morphology during oxidative degradation.

After 7 days of incubation, only slight degradation was observed, and the scaffold structure largely retained its original morphology. By day 14, degradation became more evident, as indicated by increased surface roughness and partial surface erosion, although the overall scaffold structure remained relatively intact. After 21 days, the degradation process became significantly more pronounced, with extensive structural disintegration and the formation of larger interconnected pores throughout the material.

This degradation profile demonstrates a gradual and controlled degradation process over several weeks under physiological conditions. Such behavior is highly desirable for biomedical applications that require sustained drug release, progressive tissue integration, or temporary structural support during tissue regeneration.

Enzymatic Degradation of Prepared Scaffolds

The degradation behavior of the prepared scaffolds under physiological conditions was further evaluated using a lysozyme-containing medium. Lysozyme is an enzyme naturally present in various biological fluids and is commonly used to simulate the enzymatic degradation process occurring within the human body. For this purpose, pre-weighed scaffold samples were immersed in phosphate-buffered saline (PBS) containing lysozyme at pH 7.4 and maintained at 37°C [18] (Fig. 16).

Optical microscopy observations revealed progressive enzymatic degradation of the prepared scaffolds over time. After 7 days of incubation, initial signs of degradation were observed, characterized by slight surface roughness, while the porous network structure remained largely

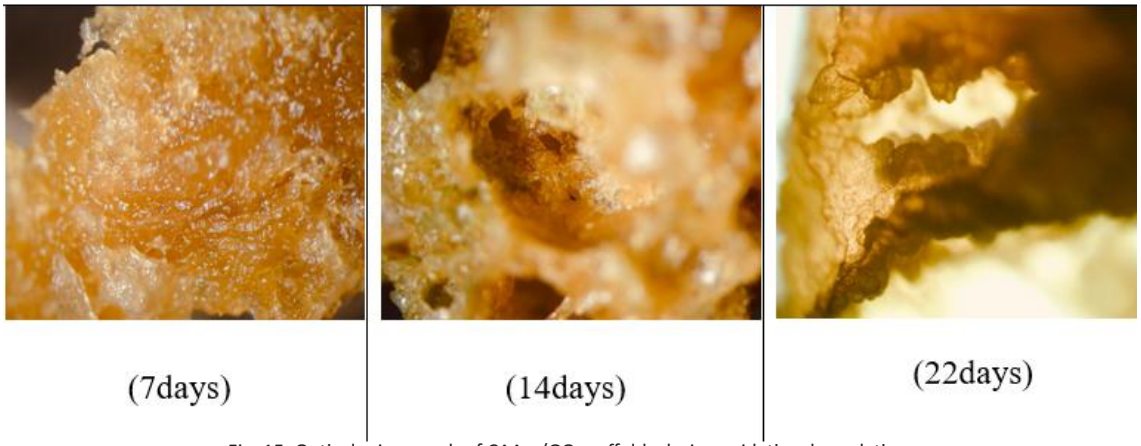


Fig. 15. Optical micrograph of CAAm/GO scaffolds during oxidative degradation.

CC BY

intact. By day 14, the degradation process became more pronounced, as evidenced by increased surface roughness and porosity. In addition, some fibers appeared thinner or partially fragmented, and larger voids developed within the network structure. After 21 days, significant degradation was detected, with extensive disintegration of the original scaffold network. Large pores and cavities were formed, and certain regions of the scaffold underwent complete degradation.

This degradation profile demonstrates a gradual breakdown of the scaffold structure over several weeks under physiological conditions, indicating its potential suitability for controlled drug release and tissue engineering applications.

The incorporation of graphene oxide significantly influenced both the degradation rate and degradation pattern of the prepared scaffolds. Based on optical microscopy observations, scaffolds containing graphene oxide exhibited slower degradation behavior compared with the pure hydrogel scaffold. Although slight surface roughness was observed after 7 days, the porous structure remained more stable and compact. By day 14, degradation became more apparent, with increased roughness and partial fragmentation of some fibers; however, the scaffold structure still retained greater integrity. After 21 days, noticeable degradation occurred, including the formation of larger pores and partial collapse of the network structure, but the extent of degradation remained lower than that observed in scaffolds without

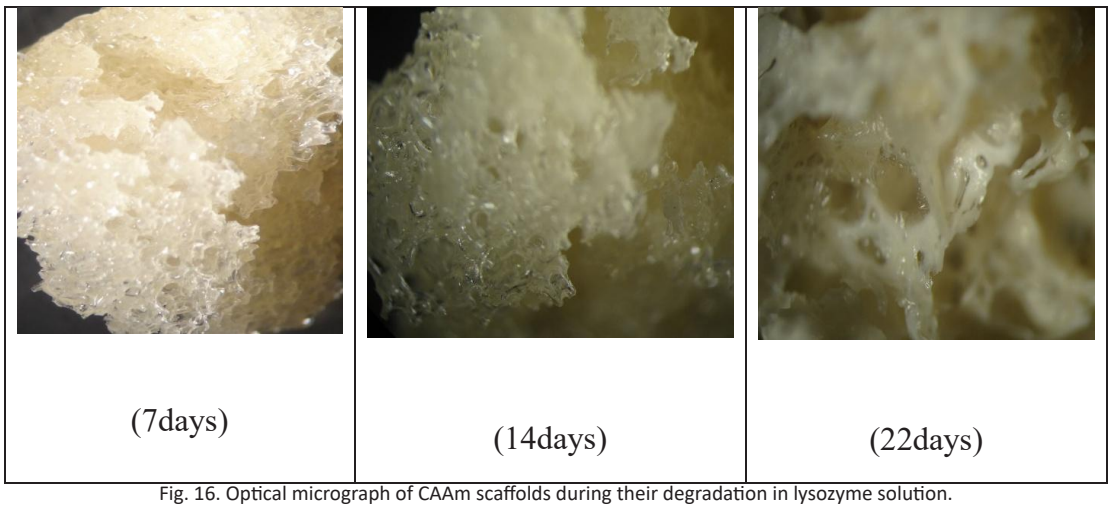


Fig. 16. Optical micrograph of CAAm scaffolds during their degradation in lysozyme solution.

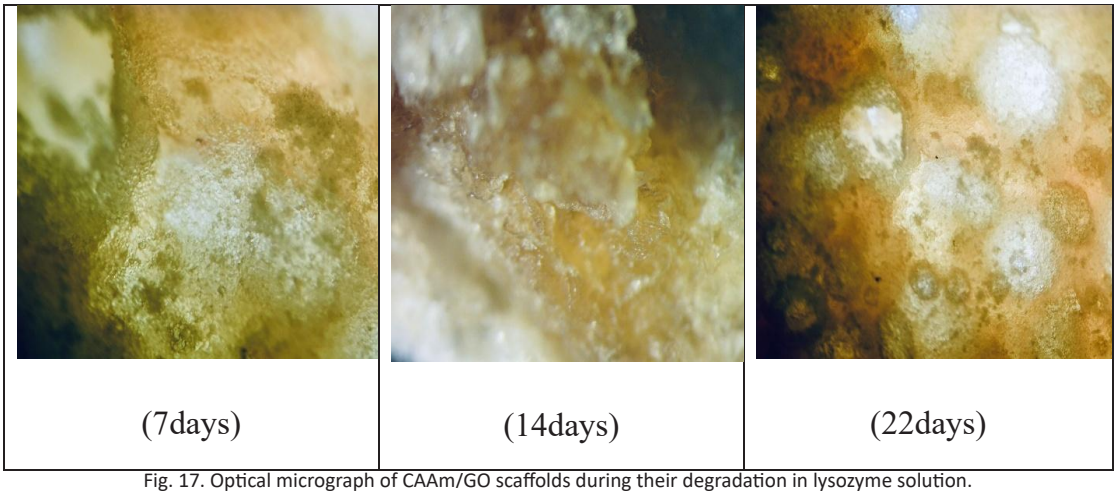


Fig. 17. Optical micrograph of CAAm/GO scaffolds during their degradation in lysozyme solution.

CC BY

graphene oxide.

The improved degradation resistance can be attributed to the enhanced cross-linking density, stronger intermolecular interactions, and increased mechanical stability introduced by graphene oxide nanosheets within the polymer matrix. Consequently, graphene oxide-containing scaffolds demonstrated a more controlled and sustained degradation behavior under physiological conditions, making them promising candidates for long-term biomedical and controlled-release applications.

These results clearly demonstrate the significant influence of scaffold composition on the degradation behavior in the presence of enzymes that simulate physiological conditions. Variations in the polymer network structure and intermolecular interactions directly affected the stability and degradation profile of the prepared scaffolds.

Furthermore, the incorporation of graphene oxide contributed to the modulation of the degradation rate by enhancing the structural integrity and stability of the polymer matrix. This effect provides a promising strategy for tailoring scaffold degradation behavior according to the requirements of specific biomedical applications, particularly in tissue engineering and controlled drug delivery systems.

CONCLUSION

In the present study, porous chitosan-based polymer scaffolds were successfully synthesized through microwave-assisted graft copolymerization of acrylamide and acrylic acid onto a chitosan backbone. The incorporation of graphene oxide into the polymeric matrix significantly enhanced the physicochemical and mechanical properties of the prepared scaffolds. FTIR analysis confirmed the successful formation of the grafted polymer network and demonstrated the existence of intermolecular interactions between graphene oxide, the polymer chains, and the loaded drug piroxicam.

The prepared scaffolds exhibited a highly porous and interconnected structure, which is favorable for water uptake, nutrient diffusion, and drug loading. Mechanical testing demonstrated that the addition of graphene oxide improved both tensile and compressive strength due to enhanced cross-linking density and stronger intermolecular interactions within the polymer matrix. However, the incorporation of graphene oxide slightly reduced scaffold porosity and swelling behavior because of increased structural compactness and reduced pore size.

In vitro drug release studies revealed that the prepared scaffolds provided sustained and controlled release of piroxicam over an extended period. The release mechanism was governed by a combination of diffusion, swelling, and polymer chain relaxation. Furthermore, graphene oxide incorporation reduced the drug release rate and enhanced release stability, indicating its important role in controlling drug diffusion within the scaffold network.

The degradation studies demonstrated gradual and controlled oxidative and enzymatic degradation under simulated physiological conditions. Scaffolds containing graphene oxide showed slower degradation rates and improved structural stability compared with pristine scaffolds, indicating enhanced resistance to degradation. This controlled degradation behavior is highly desirable for tissue engineering and long-term drug delivery applications.

Overall, the developed CAAm and CAAm/GO porous scaffolds exhibited promising structural, mechanical, swelling, degradation, and controlled drug release properties. These findings suggest that the prepared materials are promising multifunctional biomaterials for bone tissue engineering and localized controlled drug delivery applications.

CONFLICT OF INTEREST

The authors declare that there is no conflict of interests regarding the publication of this manuscript.

REFERENCES

1. Shahrezaie M, Zamanian A, Sahranavard M, Shahrezaee MH. A critical review on the 3D bioprinting in large bone defects regeneration. Bioprinting. 2024;37:e00327.
2. Babu S, Shanmugavadivu A, Selvamurugan N. Tunable mechanical properties of chitosan-based biocomposite scaffolds for bone tissue engineering applications: A review. Int J Biol Macromol. 2024;272:132820.
3. Sindhusha VB, Doraiswamy JN. The Role of Chitosan and Gelatin-Based Scaffolds in Bone Regeneration: A Systematic Review. Cureus. 2024.
4. Mukasheva F, Adilova L, Dyussenbinov A, Yernaimanova B, Abilev M, Akilbekova D. Optimizing scaffold pore size for tissue engineering: insights across various tissue types. Frontiers in Bioengineering and Biotechnology. 2024;12.
5. Zhu T, Zhou H, Chen X, Zhu Y. Recent advances of responsive scaffolds in bone tissue engineering. Frontiers in

CC BY

Bioengineering and Biotechnology. 2023;11.
6. Abbadessa A, Ronca A, Salerno A. Integrating bioprinting, cell therapies and drug delivery towards in vivo regeneration of cartilage, bone and osteochondral tissue. Drug Delivery and Translational Research. 2023;14(4):858-894.
7. Abpeikar Z, Javdani M, Mirzaei SA, Alizadeh A, Moradi L, Soleimannejad M, et al. Macroporous scaffold surface modified with biological macromolecules and piroxicam-loaded gelatin nanofibers toward meniscus cartilage repair. Int J Biol Macromol. 2021;183:1327-1345.
8. Kashte SB, Kadam S, Maffulli N, Potty AG, Migliorini F, Gupta A. Osteoinductive potential of graphene and graphene oxide for bone tissue engineering: a comparative study. J Orthop Surg Res. 2024;19(1).
9. Vu QL, Chiu IH, Do LT, Nguyen TP-Q, Nguyen TH, Thanh DV, et al. Development of an injectable thermosensitive hydrogel depot system for controlled and sustained subcutaneous drug delivery. International Journal of Pharmaceutics: X. 2026;11:100529.
10. Ofokansi KC, Adikwu MU. Formulation and Evaluation of Microspheres Based on Gelatin-Mucin Admixtures for the Rectal Delivery of Cefuroxime Sodium. Tropical Journal of Pharmaceutical Research. 2007;6(4).
11. Oh S, Stache EE. Recent advances in oxidative degradation of plastics. Chem Soc Rev. 2024;53(14):7309-7327.
12. Suresh V, Shams R, Dash KK, Shaikh AM, Béla K. Comprehensive review on enzymatic polymer degradation: A sustainable solution for plastics. Journal of Agriculture and Food Research. 2025;20:101788.
13. Thirumalesh Chevala N, Muthuramalingam S, Kumar L, Mallikarjuna Rao C. Nanoporous scaffold fabrication for biomedical application by employing probe sonication. Materials Today: Proceedings. 2022;55:94-97.
14. Himawan A, Korelidou A, Pérez-Moreno AM, Paris JL, Dominguez-Robles J, Vora LK, et al. Formulation and evaluation of PVA-based composite hydrogels: physicochemical, leachables, and in vitro immunogenicity studies. Journal of Materials Chemistry B. 2025;13(7):2431-2445.
15. Ilić-Stojanović S, Nikolić L, Nikolić V, Ristić I, Cakić S, Petrović SD. Biomedical Applications of Thermosensitive Hydrogels for Controlled/Modulated Piroxicam Delivery. Gels. 2023;9(1):70.
16. Schiavi A, Cuccaro R, Troia A. Functional mechanical attributes of natural and synthetic gel-based scaffolds in tissue engineering: strain-stiffening effects on apparent elastic modulus and compressive toughness. J Mech Behav Biomed Mater. 2022;126:105066.
17. Tajvar S, Hadjizadeh A, Samandari SS. Scaffold degradation in bone tissue engineering: An overview. International Biodeterioration and Biodegradation. 2023;180:105599.
18. Al-Arjan WS, Aslam Khan MU, Nazir S, Abd Razak SI, Abdul Kadir MR. Development of Arabinoxylan-Reinforced Apple Pectin/Graphene Oxide/Nano-Hydroxyapatite Based Nanocomposite Scaffolds with Controlled Release of Drug for Bone Tissue Engineering: In-Vitro Evaluation of Biocompatibility and Cytotoxicity against MC3T3-E1. Coatings. 2020;10(11):1120.

CC BY